International Journal of Heat and Mass Transfer 194 (2022) 123058

Contents lists available at ScienceDirect

International Journal of Heat and Mass Transfer

journal homepage: www.elsevier.com/locate/hmt

Wettability and evaporation of dilute sodium dodecyl sulfate droplets on micropillar-arrayed non-wetting surfaces

Guo-Hao Li[a], Xiao-Ye Yang[a], Xianfu Huang[b,c,*], Ying-Song Yu[a,*]

[a] Department of Mechanics, School of Civil Engineering, Architecture and Environment, Hubei University of Technology, Wuhan 430068, PR China
[b] State Key Laboratory of Nonlinear Mechanics, Institute of Mechanics, Chinese Academy of Sciences, Beijing 100190, PR China
[c] School of Engineering Science, University of Chinese Academy of Sciences, Beijing 100049, PR China

ARTICLE INFO

Article history:
Received 6 April 2022
Revised 18 May 2022
Accepted 20 May 2022
Available online 7 June 2022

Keywords:
Droplet
Sodium dodecyl sulfate
Evaporation
Polydimethylsiloxane
Contact angle
Contact radius
Spreading

ABSTRACT

Wettability and evaporation of dilute sodium dodecyl sulfate (SDS) droplets on micropillar-arrayed polydimethylsiloxane (PDMS) were experimentally studied. It was found that the apparent, advancing and receding contact angles all decreased with the increase of initial SDS concentration and wettability of dilute SDS droplets depended on both SDS concentration and surface roughness. Due to the adhesion between the droplets and the micropillars, all evaporation began with constant contact radius (CCR) mode. It is more interesting that short-time spontaneous spreading was found to follow the CCR stage for dilute SDS droplets evaporating on the patterned surface with sparser micropillars, which can be attributed to the transition from the Cassie-Baxter wetting state to the Wenzel wetting state (CB-W transition). Such a transition has been experimentally observed and a theoretical model was developed to qualitatively elucidate the spontaneous spreading.

1. Introduction

Evaporation of a sessile droplet on a solid surface is a ubiquitous phenomena and has been found wide applications in fields such as microfluidics, ink-jet print, lab-on-a-chip, pesticide spraying and energy harvest [1–6]. For pure water droplets, the evaporation usually starts with the constant contact radius (CCR) mode characterized with pinned contact line due to contact angle hysteresis and decreasing contact angle, then switches to the constant contact angle (CCA) mode characterized with nearly unchanged instantaneous contact angle and receding of the contact line, and finally completes with the decrease of both the contact radius and the contact angle [7]. During the latest decades, evaporation of single- and multi-component sessile droplets has been broadly investigated from experiments, theory, and numerical simulation. And it is found that evaporation of a sessile droplet can be influenced by a lot of factors such as the physical and chemical properties of liquid [8,9], surface roughness of substrates [10–13], surface wettability [14–16], substrate temperature [17–18], substrate elasticity [19–21], thermal conductivity of substrates [22,23], the application of external field [24,25], and ambient environment [26,27].

Surfaces constructed with micro/nano-structures are usually more hydrophobic or hydrophilic [28–30]. If the cavities between micro-/nano-pillars or micro-/nano-pores is fully filled with liquid, the droplet is in the Wenzel (W) wetting state. In this case, surface roughness makes a hydrophilic surface more hydrophilic while makes a hydrophobic surface more hydrophobic [31]. If the liquid just sits on the top of these surfaces, in other words, the liquid can not contact with the bottom of the cavities, and the droplet is in the Cassie-Baxter (CB) wetting state [32]. Because of the existence of air between the liquid and the bottom of the cavities, it becomes more feasible to obtain a superhydrophobic surface. It should be noted that the pure CB and W wetting states are rare in occurrence [33,34]. However, since there is an energy barrier between the two wetting states, the wetting state of a droplet might switch from the CB wetting state to the W wetting state through the application of an external pressure [28,35], vibration [36] and surface acoustic waves [37], etc. The CB-W transition will limit the application of superhydrophobic surfaces. For the evaporation of sessile droplets on rough surface, such a CB-W transition can also be observed [38–40].

Surfactants also have an important influence on the evaporation of sessile droplets. It was found that surfactant concentration of a sessile droplets containing soluble surfactants had no significant

* Corresponding authors.
E-mail addresses: huangxf@imech.ac.cn (X. Huang), yuys@hbut.edu.cn (Y.-S. Yu).

https://doi.org/10.1016/j.ijheatmasstransfer.2022.123058
0017-9310/

effect on the evaporation rate, [41,42] but this was the exception for insoluble surfactants [43]. In 2019, Kwieciński et al. [44] found that the contact angle of dilute SDS droplets with an initial SDS concentration below 0.5 critical micelle concentration (CMC) underwent a process of decreasing, increasing, and decreasing again during the evaporation process, resulting in the smallest local contact angle. They also found that the bulk SDS concentration at the local contact angle minimum decreased with the decrease of initial SDS concentration. In contrast, Akanno et al. [45] found that CCA stage was never observed during the evaporation due to the pinning effect of surfactant solution droplets on the formed coffee ring. Marin et al. [46] found that different types of surfactants could stiffen or elasticize the surface of droplets, thereby changing the fluid flow of evaporation and enhancing the classic coffee ring effect or causing full flow reversal. Karapetsas et al. [47] revealed that droplet lifetime is significantly affected by the balance between surfactant-enhanced spreading, inhibiting motion induced by thermal Marangoni stress, and hindering evaporative flux by reducing the effective interfacial area. Recently, Aldhaleai and Tsai [48] studied the evaporation of aqueous didodecyldimethylammonium bromide sessile droplets on a superhydrophobic surface constructed with micropillars, and found that the adsorption of this surfactant on the interface could destruct the CB wetting state of the droplets to the W wetting state at a higher initial surfactant concentration, resulting in the difference in the evaporation characteristics of surfactant-laden droplets. However, to our best knowledge there are no reports on the evaporation of sessile SDS-laden droplets evaporating on a hydrophobic surface constructed with micropillars up till now. Is there a CB-W transition during the evaporation and what is the influence of initial SDS concentration on the evaporation characteristics?

In this work, wettability and evaporation of dilute SDS droplets on micropillar-arrayed PDMS surfaces with square lattices was experimentally studied. It was found that (i) the apparent, advancing and receding contact angles all decreased with increasing initial SDS concentration; (ii) surface roughness and initial SDS concentration had great influence on surface wettability; (iii) a short-time spontaneous spreading process was observed for dilute SDS droplets evaporating on the surfaces with sparser micropillars at a certain range of initial SDS concentration, which can be attributed to the CB-W transition and the spreading appeared earlier for droplets with a greater initial SDS concentration.

2. Materials and methods

PDMS (Dowsil^{TM} 184, Dow Europe GMBH C/O Dow Silicones Deutschland GMBH, Germany, mass ratio of base to curing agent was 10:1) surfaces with circular micro-cylinder arrays were fabricated using the peeling-off method [9,13]. The diameter d and height H of micro-cylinder were both fixed at 20 μm and the cylinder-to-cylinder spacing w was 5, 20 and 50 μm, respectively. Figue 1 shows the characterization of these micropillar-arrayed PDMS surfaces by a scanning electronic microscopy (SEM, FEI Quanta 200 FEG, Nederland). Solid fraction $\phi = \frac{\pi d^2}{4(w+d)^2}$ and surface roughness $R_f = 1 + \frac{\pi dH}{(w+d)^2}$ were used for characterizing these surfaces. The values of ϕ for the three MICROPATTERNED surfaces are 0.50, 0.20 and 0.06, respectively. And the corresponding values of R_f are 3.01, 1.79 and 1.26, respectively.

SDS with purity greater than 99% (Aldrich-Sigma, China) was dissolved in deionized water to obtain dilute SDS solutions with SDS concentrations of 0.05, 0.1, 0.2, 0.3, 0.5, 0.8 and 1.0 CMC. Wettability of dilute SDS droplets including the apparent (θ_e), advancing (θ_a) and receding (θ_r) contact angles was measured using a droplet shape analyzer (DSA30, Krüss, Germany). Because the surface tension of SDS solutions is relatively low and the adhesion between droplets and the surfaces is very small, SDS droplets were all gentelly deposited on these surfaces using a NE30 needle. θ_e was measured by capturing the images of SDS droplets with a nominal volume of 2.0 μL on horizontal surfaces. Contact angle hysteresis was characterized using the sliding (S) method by tilting these surfaces at a tilting speed of 30° per minute [49–53]. The values of θ_a and θ_r were obtained from the images at the instant when dilute SDS droplets with a nominal volume of 8.0 μL (the initial SDS concentration was 0.05, 0.1, 0.2, 0.3, and 0.5 CMC) began to move downward. Contact angle hysteresis of dilute SDS droplets with initial SDS concentrations of 0.05, 0.1, 0.2, 0.3, 0.5, 0.8 and 1.0 CMC was measured using the injection-retraction (IR) method following the procedure suggested by Huhtamäki et al. [54]. Besides, pressing a sessile droplet with a plate can also be used for the determination of contact angle hysteresis [55]. SDS droplets with a nominal volume of 1.0 μL were slightly deposited on these surfaces using a NE30 needle and recorded with the DSA 30 droplet shape analyzer at the speed of 0.5 fps as soon as possible to record the evaporation. The ambient temperature and relative humidity were 23±1 °C and 48±3%, respectively. Each experiment was repeated at least three times to ensure the reproductivity.

Table 1
Analysis on wettability of dilute SDS droplets on micropillar-arrayed PDMS surfaces.

ϕ	c_{SDS} (CMC)	θ_e	θ_W	θ_{CB}	θ_a	θ_r
0.50	0.05	130°±2°	169°±2°	131°±2°	140°±2°	118°±2°
	0.1	127°±2°	146°±2°	129°±2°	140°±2°	117°±2°
	0.2	126°±2°	137°±2°	128°±2°	138°±2°	116°±2°
	0.3	123°±2°	133°±2°	128°±2°	136°±2°	115°±2°
	0.5	121°±2°	111°±2°	124°±2°	131°±2°	108°±2°
	0.8	116°±2°	96°±2°	121°±2°	129°±2°	105°±2°
	1.0	115°±2°	72°±2°	116°±2°	128°±2°	100°±2°
0.20	0.05	142°±2°	125°±2°	150°±2°	149°±2°	136°±2°
	0.1	141°±2°	119°±2°	149°±2°	148°±2°	134°±2°
	0.2	140°±2°	115°±2°	148°±2°	147°±2°	131°±2°
	0.3	139°±2°	114°±2°	148°±2°	145°±2°	130°±2°
	0.5	136°±2°	102°±2°	145°±2°	144°±2°	126°±2°
	0.8	131°±2°	94°±2°	144°±2°	142°±2°	119°±2°
	1.0	129°±2°	79°±2°	141°±2°	140°±2°	113°±2°
0.06	0.05	149°±2°	114°±2°	163°±2°	155°±2°	147°±2°
	0.1	147°±2°	110°±2°	162°±2°	153°±2°	146°±2°
	0.2	146°±2°	108°±2°	162°±2°	151°±2°	144°±2°
	0.3	144°±2°	106°±2°	162°±2°	148°±2°	141°±2°
	0.5	143°±2°	99°±2°	161°±2°	147°±2°	139°±2°
	0.8	99°±2°	92°±2°	160°±2°	109°±2°	46°±2°
	1.0	96°±2°	82°±2°	158°±2°	107°±2°	44°±2°

3. Results and discussion

3.1. Wettability of dilute SDS droplets on micropillar-arrayed non-wetting surfaces

Table 1 lists the apparent, advancing, and receding contact angles of dilute SDS droplets on micropillar-arrayed PDMS surfaces. The advancing, and receding contact angles were obtained from the images (as shown in Fig. 2) at the instant when the droplets began to move downward. When characterizing the wettability of a sessile droplet on a rough surface, there are mainly four models to our best knowledge. If the rough surface is wetted by liquid without the existence of air between the liquid and the surface, the apparent contact angle can be determined by the W model [31]: $\cos\theta_W = R_f \cos\theta_Y$, where θ_W and θ_Y are Wenzel's contact angle and the intrinsic contact angle of a sessile droplet on an ideally smooth solid surface. If there is no penetration of liquid into the cavities on rough surface, the apparent contact angle can be determined by the CB model [32]: $\cos\theta_{CB} = \phi\cos\theta_Y - (1-\phi)$, where θ_{CB} is the Cassie's contact angle. In 2005, Zheng et al. [56]

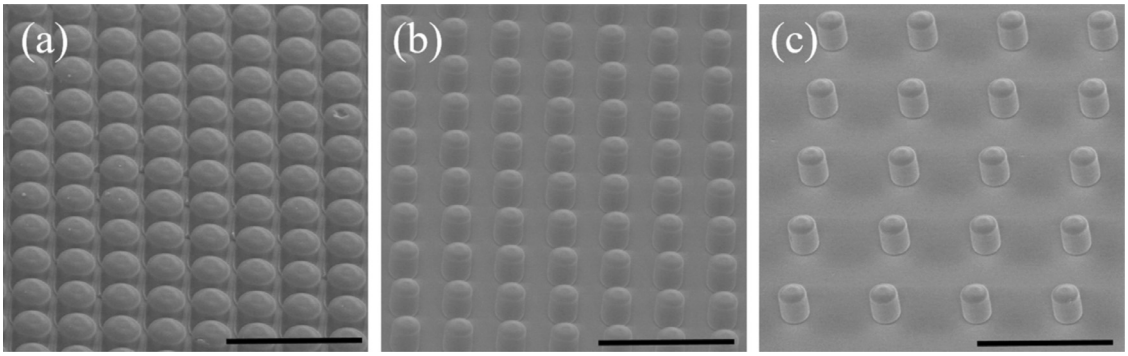

Fig. 1. SEM characterization of micropillar-arrayed PDMS surfaces. (a) ϕ=0.50, (b) ϕ=0.20, (c) ϕ=0.06.

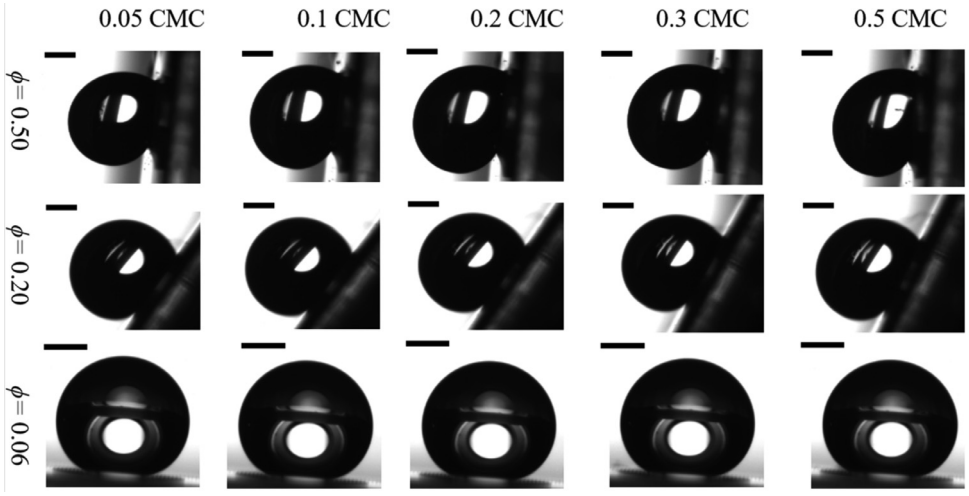

Fig. 2. Images for measuring contact angle hysteresis of dilute SDS droplets on micropillar-arrayed PDMS surfaces. All inserted scale bars represent 1 mm.

developed a mixed wetting model and the apparent contact angle is given as: $\cos\theta_e = \chi\cos\theta_W + (1-\chi)\cos\theta_{CB}$, where χ is a parameter denoting the fraction of the surface which has transitioned to the W wetting state while the other part of the surface is still Cassie-Baxter-wetted. Later, Liu et al. proposed the triple line pinning model [57]. In this work, the former three wetting models were used to analyze the wettability of SDS droplets on these micropillar-arrayed PDMS surfaces. The values of the apparent contact angles of dilute SDS droplets with SDS concentrations of 0.05, 0.1, 0.2, 0.3, 0.5, 0.8 and 1.0 CMC on a common PDMS surface at temperature of 23±1 °C and relative humidity of 48±3% were 109°±2°, 106°±2°, 104°±2°, 103°±2°, 97°±2°, 92°±2° and 84°±2°, respectively. Substituting these values into the W and CB wetting models, the values of θ_W and θ_{CB} were obtained, as listed in Table 1. On the patterned surface with a solid fraction of 0.50, the apparent contact angles of dilute SDS droplets were approximately equal to the Cassie's contact angle when the initial SDS concentration was no more than 0.5 CMC, indicating that these droplets were all in the CB wetting state. For the case of dilute SDS droplets with initial SDS concentrations of 0.8 and 1.0 CMC, the apparent contact angles were both much larger than the Wenzel's contact angle while slightly less than the Cassie's contact angles, demonstrating that the droplets were all in CB-like wetting state. On the patterned surface with a solid fraction of 0.20, the apparent contact angles were all much larger than the Wenzel's contact angle while several or ten degrees less than the Cassie's contact angles, which indicated the droplets were likely in the composite wetting state [58]. As cylinder-to-cylinder spacing increased to 50 μm (the solid fraction is 0.06), the apparent contact angles of aqueous SDS droplets with SDS concentration no more than 0.5 CMC were all about no more than twenty degrees less than the Cassie's contact angle while more than 30° larger than the Wenzel's contact angle, indicating the droplets were more likely in the CB or composite wetting state [58]. However, when SDS concentration was 0.8 or 1.0 CMC, the apparent contact angles were both slightly larger than the Wenzel's contact angle, suggesting the droplets were nearly in the W wetting state. The wettability of dilute SDS droplets on micro-patterned PDMS surfaces can also be concluded from contact angle hysteresis for a Cassile-like wetting is characterized by low contact angle hysteresis while a Wenzel-like wetting is related with high contact angle hysteresis [28,58]. As shown in Table 1, the values of contact angle hysteresis for both CB and Cassie-like wetting state were all much less than those for Wenzel-like wetting state.

Contact angle hysteresis of dilute SDS droplets with an initial SDS concentration no more than 0.5 CMC on micropillar-arrayed PDMS surfaces was obtained from the images when these droplets start to slide on inclined surfaces, as shown in Fig. 2. From Fig. 2, it was easily found that as the solid fraction decreased, the adhesion between the micropillars and the droplet is weaken, and thus the droplets could slide more easily on sparser micropillars, which can be concluded from the case of a much less inclination angle on surfaces with sparser micropillars. The values of the advancing and receding contact angles were all listed in Table 1. From Table 1, it was found that both the advancing and receding contact angles decreased with increasing initial SDS concentration. On the patterned surface with a solid fraction of 0.50 or 0.20, there was a slight decrease of advancing and receding contact angles. When the solid fraction of a patterned surface decreased to 0.06, both the advancing and receding contact angles decreased slightly with the in-

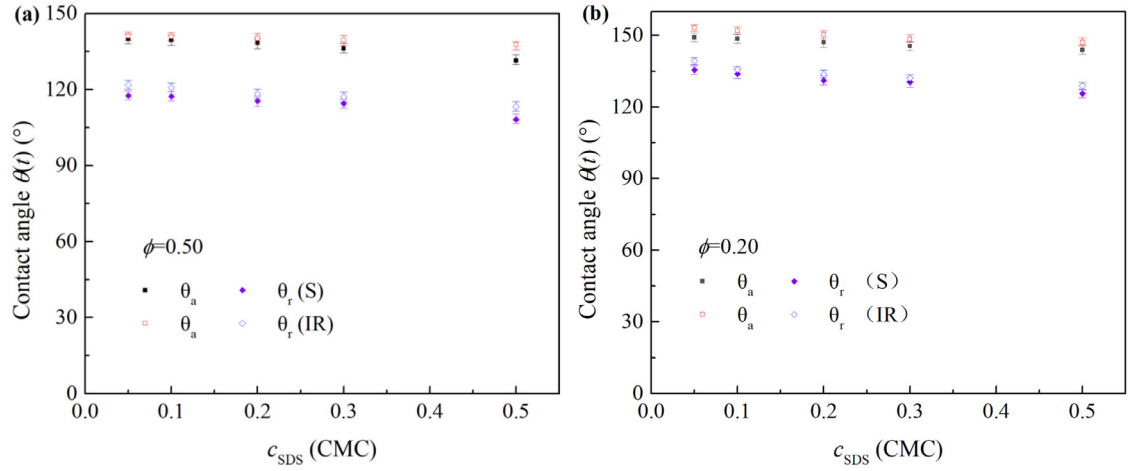

Fig. 3. Contact angle hysteresis of aqueous SDS droplets on micropillar-arrayed PDMS surfaces with different solid fractions. (**a**) ϕ=0.50, (**b**) ϕ=0.20.

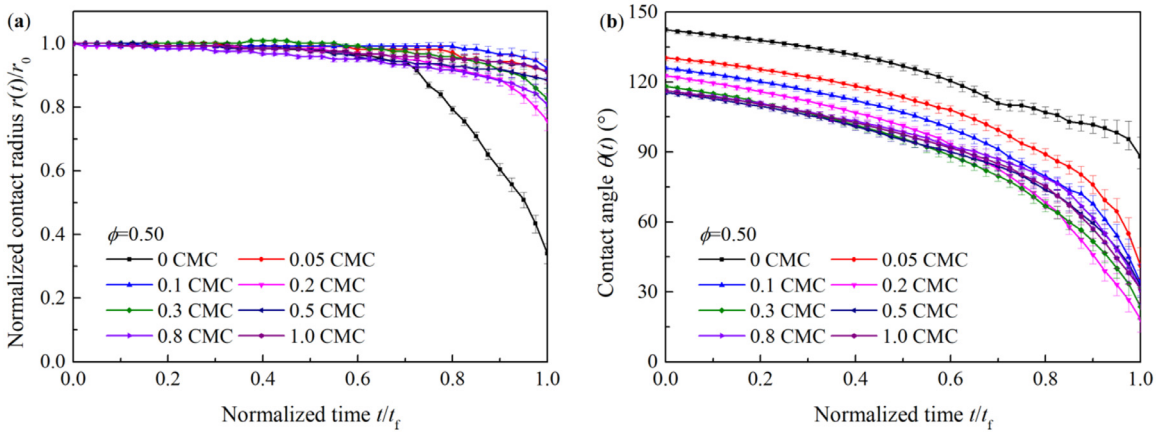

Fig. 4. Evaporation curves of dilute SDS droplets with different initial SDS concentrations on a micropillar-arrayed PDMS surface with a solid fraction of 0.50. (**a**) normalized contact radius, (**b**) contact angle.

crease of initial SDS concentration when initial SDS concentration was no more than 0.5 CMC. However, when the initial SDS concentration was 0.8 CMC, both the advancing and receding contact angles were much less than the corresponding values of dilute SDS droplets with an initial SDS concentration of 0.5 CMC. And there were little differences in both the advancing and receding contact angles of dilute SDS droplets with initial SDS concentrations of 0.8 CMC and 1.0 CMC, respectively. Figure 3 shows the comparison between the advancing and receding contact angles obtained using the S metho and those using the IR method. From Fig. 3, it can be concluded that there was no obvious difference. Contact angle hysteresis of dilute SDS droplets on microtextured PDMS surface with a solid fraction of 0.06 can not be measured using the IR method because the droplets could easily move on the surface during the insertation of a neddle into the droplets.

3.2. Evaporation of dilute SDS droplets on micropillar-arrayed non-wetting surfaces

Figures 4-6 show the evolution of normalized contact radius (ratio of the instantaneous contact radius $r(t)$ to the initial contact radius r_0) and instantaneous contact angle $\theta(t)$ of evaporating sessile dilute SDS droplets on micropillar-arrayed PDMS surfaces versus normalized time t/t_f, where t_f is the total evaporation time. The curves of pure water droplets on these micropillar-arrayed PDMS surfaces were extracted from Ref. [13] (the environmental temperature and relative humidity were 26.5 °C ±1 °C and 52 ± 2%, respectively). Compared with pure water droplet, aqueous SDS droplets had a much different evaporation characteristics. On the patterned surface with a solid fraction of 0.50 (Fig. 4), the evaporation always began with the CCR mode no matter what the initial SDS concentration was. And the CCR stage dominated about 80% of the total evporation time for dilute SDS droplets with initial SDS concentrations of 0.05 and 0.1 CMC. As more SDS molecules were introduced into the droplet, the duration of the CCR stage became shorter and pinning-depinning behaviors of the contact line were easily observed, as shown in Fig. 4(a). For the case of dilute SDS droplets with initial SDS concentration ranging from 0.2 to 1.0 CMC evaporating on this surface, it seemed that the normalized contact radius at the normalized time interval bwteeen 0.6 and 1.0 would increase with the initial SDS concentration. However, as shown in Fig. 4(a), an inverse relationship was observed, which might be attributed to the deformation of micropillars due to surface tension and Laplace pressue. Moreover, local wettability of SDS solutions on micropillars as well as the adsorption of SDS molecules on micropillars also played important roles and should be studied further. On the patterned surface with a solid fraction of 0.20 (Fig. 5), the evaporation also exhibited with the CCR mode and the duration of the CCR stage were very long for dilute SDS droplets with initial SDS concentrations of 0.05, 0.1 and 0.2 CMC. For the case of dilute SDS droplets with initial SDS concentrations of 0.3 and 0.5 CMC, the durations of the

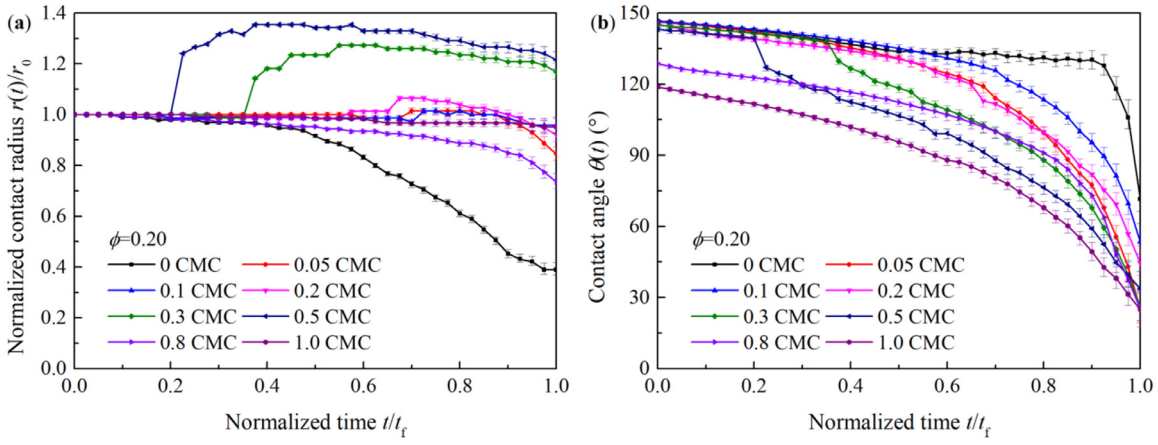

Fig. 5. Evaporation curves of dilute SDS droplets with different initial SDS concentrations on a micropillar-arrayed PDMS surface with a solid fraction of 0.20. (**a**) normalized contact radius, (**b**) contact angle.

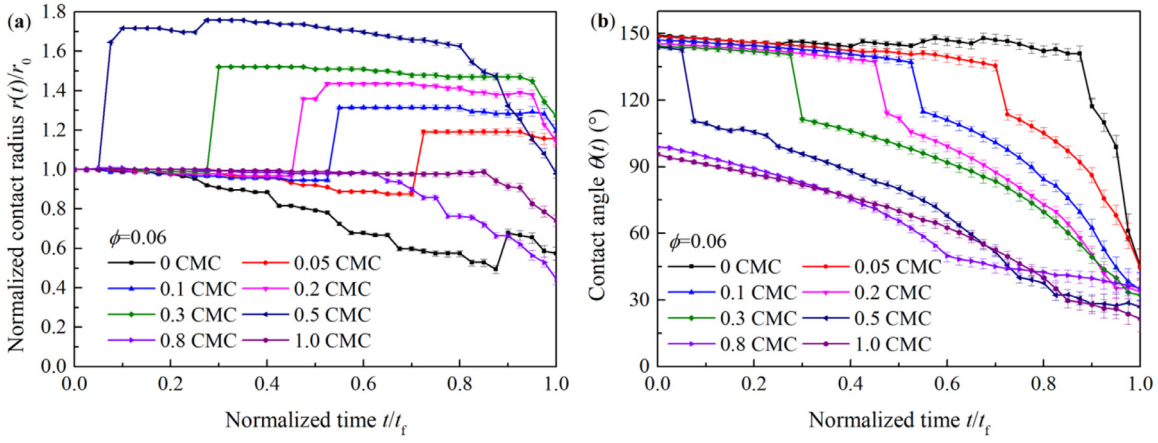

Fig. 6. Evaporation curves of dilute SDS droplets with different initial SDS concentrations on a micropillar-arrayed PDMS surface with a solid fraction of 0.06. (**a**) normalized contact radius, (**b**) contact angle.

CCR stage were 35% and 20% of the total evaporation time, respectively. Following the CCR stage, the droplet spontaneously spread for a relatively long time. Once the contact radius reached its maximum, it was pinned again for some time. On the patterned surface with a solid fraction of 0.06 (Fig. 6), short-time spontaneous spreading was observed following the CCR stage during the evaporation of dilute SDS droplets with initial SDS concentrations of 0.05, 0.1, 0.2, 0.3 and 0.5 CMC. And the duration of the first CCR stage became shorter and the spontaneous spreading occured earlier as the initial SDS concentration increased. When the droplet spontaneously spread on the surface, the contact angle decreased sharply from about 140° to about 115°, as shown in Fig. 6(b). Once the instantaneous contact radius reached its maximum, the contact radius was nearly unchanged for a long time. However, when the initial SDS concentration was 0.8 or 1.0 CMC, a long-time CCR stage was observed and the duration of the CCR stage of a dilute SDS droplet with an initial SDS concentration of 1.0 CMC was longer than that with the initial SDS concentration of 0.8 CMC.

In our previous experiments, it was found that dilute SDS droplets could spontaneously spread for a short time at the early age of the evaporation process. However, as shown in Figs. 4-6, the evaporation of dilute SDS droplets all began with the CCR mode, which can be attributed to the contribution of surface roughness to the adhesion between patterned surfaces and the droplets due to the existence of micropillars.

Figure 7 lists the images extracted from the videos of dilute SDS droplets on the patterned surface with a solid fraction of 0.06. From Fig. 7, when a dilute SDS droplet with the initial SDS concentration of no more than 0.5 CMC was slightly deposited on the surface, there was usually a visible gap between the droplet and the patterned surface, indicating that the droplet was in the CB or composite wetting state. As water evaporated from the liquid-vapor interface, the instantaneous SDS concentration increased and the penetration of liquid into the cavities between micropillars became easier. As shown in the enlarged images in Fig. 7, it was found that the filling of mixtures with liquid was a quasi-static process and the filling became more easily as the initial SDS concentration increased. Hence, the wetting state gradually changed from the CB state to the W state. With the transition of the wetting state, there was a sudden increase of contact radius and a sharp decrease of contact angle. As a contrast, some images of an evaporating dilute SDS droplet with an initial SDS concentration of 0.8 CMC were also given in Fig. 7. For this case, it was found there was no visible gap between the droplet at the first time, indicating that the droplet was in the W wetting state. Because the cavities between micropillars were almost fully filled with liquid, the adhesion between the droplet and the surface was very strong, resulting in the pinning of the contact line. On the other hand, though the instantaneous SDS concentration increased with the loss of water, there was only a slight decrease of surface tension of the liquid and solid-vapor interfacial tension. Thus, there was not enough

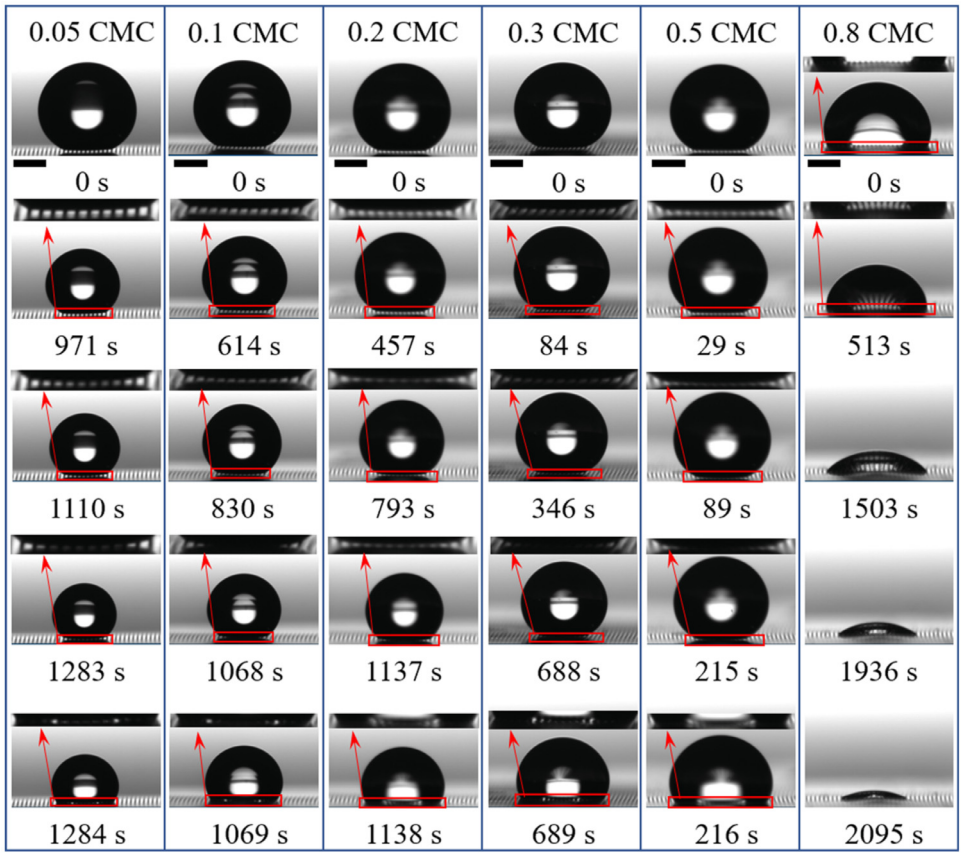

Fig. 7. Snapshots of evaporating dilute SDS droplets on the micropillar-arrayed PDMS surface with a solid fraction of 0.06. All inserted scale bars represent 500 μm.

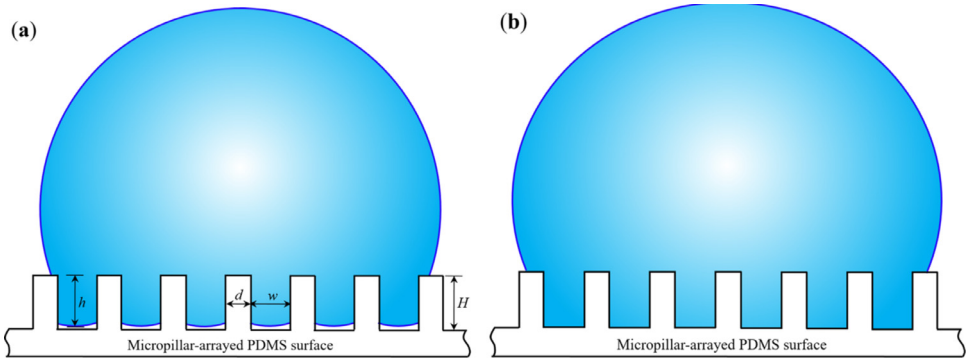

Fig. 8. Mechanism for spontaneous spreading. (a) schematics of wetting state just before the occurrence of spontaneous spreading, (b) schematics of Wenzel wetting state with pinned contact line.

excess surface energy to overcome the energy barrier due to contact angle hysteresis. Therefore, there was no spontaneous spreading for this case.

To eludicate the short-time spreading of dilute SDS droplets with a certain range of initial SDS concentration on patterned surfaces with sparser micropillars, a simple model based on energy analysis was developed here. Based on experimental observation, as shown in Fig. 7, we assume at the instant just before spontaneous spreading the droplet has a contact radius of r and a contact angle of θ, and liquid nearly contacts with the bottom in the cavities between micropillars, viz., the penetration height h is very close to the pillar height H, as shown in Fig. 8(a). The total surface energy E can be expressed as [58,59]

$$E = \gamma_{lv}^{(1)} A_{lv}^{(1)} + \gamma_{lv}^{(2)} A_{lv}^{(2)} + \gamma_{sv} A_{sv} + \gamma_{sl}\left(\phi \pi r^2 + 2\pi r h\right) \quad (1)$$

where $\gamma_{lv}^{(1)}$, $\gamma_{lv}^{(2)}$, γ_{sv} and γ_{sl} are the liquid-vapor interfacial tension of liquid above the top surface of the patterned substrate, the liquid-vapor interfacial tension of liquid between micropillars, the solid-vapor interfacial tension and the solid-liquid interfacial tension, respectively. $A_{lv}^{(1)}$, $A_{lv}^{(2)}$ and A_{sv} are the liquid-vapor area of liquid above the top surface of the patterned substrate, the liquid-vapor area of liquid between micropillars and the solid-vapor area, respectively.

After about 1 s (as shown in the last two subimages of the former five sequences in Fig. 7), the cavities between micropillars are fully filled with water, viz., the droplet is now in the W wetting state, as shown in Fig. 8(b). During this process, evaporation loss of water and excess liquid penetration are both negligible. Suppose the contact line is still pinned, thus the liquid-vapor interfacial area above the contact line will not vary. And the liquid-vapor

interface between micropillars and the solid-vapor interface will be replaced by solid-liquid interface. Thus, the difference in the total surface energy between the two instants can be expressed as

$$\Delta E = E_1 - E_2 = (1-\phi)\pi r^2\left(\gamma_{lv}^{(2)} + \gamma_{sv} - \gamma_{sl}\right) = (1-\phi)\pi r^2\gamma_{lv}^{(2)}(1+\cos\theta_Y) \quad (2)$$

where E_1 and E_2 represent the total surface energy of the system at the instant just before spontaneous spreading and that when the droplet is in the W wetting state with pinned contact line. θ_Y is the Young's contact angle of a dilute SDS droplet having the same SDS concentration as that of the liquid between the micropillars on a smooth planar PDMS surface. From Eq. (2), it can be concluded that $\Delta E > 0$, indicating that if the excess surface energy is enough to overcome the energy barrier due to contact angle hysteresis, the droplet can spontaneously spread on the surface. It should be noted that more theoretical analysis for spontaneous spreading should be studied by taking into account surface tension and Laplace pressure [60]. However, as the droplets evaporated, the instantaneous SDS concentration would increase, resulting in decreasing surface tension and Laplace pressure. Hence, currently it is still a great challenge to study the filling of microtextures with liquid from a microscopic view.

4. Conclusion

Wettability of dilute SDS droplets on micropillar-arrayed PDMS surfaces with different solid fraction were experimentally investigated. The apparent, advancing and receding contact angles were found to decrease with the increase of initial SDS concentration and increase with the decrease of solid fraction when the initial SDS concentration was no more than 0.5 CMC. For dilute SDS droplets with initial SDS concentration of 0.8 or 1.0 CMC, the apparent, advancing and receding contact angles of the droplets on a patterned surface with a solid fraction of 0.20 were the greatest as compared to the other two patterned surfaces.

Evaporation of dilute SDS droplets on these patterned surfaces was also conducted. It was found the evaporation usually began with the CCR stage no matter what the initial SDS concentration was. Short-time spontaneous spreading was observed to follow the CCR stage for dilute SDS droplets with a certain range of initial SDS concentration evaporating on the patterned surface with sparser micropillars. On this patterned surface, the short-time spontaneous spreading was found to begin earlier with the increase of the initial SDS concentration. Further analysis showed such a spontaneous spreading could be attributed to the CB-W transition.

Declaration of Competing Interest

There are no conflicts of interest to declare.

CRediT authorship contribution statement

Guo-Hao Li: Investigation, Writing – original draft, Writing – review & editing, Data curation. **Xiao-Ye Yang:** Writing – review & editing, Data curation. **Xianfu Huang:** Writing – review & editing, Conceptualization, Funding acquisition. **Ying-Song Yu:** Supervision, Writing – review & editing, Conceptualization, Funding acquisition.

Acknowledgments

This work was jointly supported by the National Natural Science Foundation of China (Grant Nos.: 11572114), the PetroChina Innovation Foundation (Grant No.: 2019D-5007-0102) and the Chinese Academy of Sciences Key Research Program of Frontier Sciences (Grant No.: QYZDJ-SSW-JSC019).

References

[1] D. Bonn, J. Eggers, J. Indekeu, J. Meunier, E. Rolley, Wetting and spreading, Rev. Mod. Phys. 81 (2) (2009) 739–805.
[2] D. Brutin, V. Starov, Recent advances in droplet wetting and evaporation, Chem. Soc. Rev. 47 (2) (2018) 558–585.
[3] H.Y. Erbil, Evaporation of pure liquid sessile and spherical suspended drops: a review, Adv. Colloid Interf. Sci. 170 (2012) 67–86.
[4] D.Y. Zang, S. Tarafdar, Y.Y. Tarasevich, M.D. Choudhury, T. Dutta, Evaporation of a droplet: from physics to applications, Phys. Rep. 804 (2019) 1–56.
[5] Y.P. Zhao, Physical Mechanics of Surfaces and Interfaces, Science Press, Beijing, 2012.
[6] G.B. Xue, Y. Xu, T.P. Ding, J. Li, J. Yin, W.W. Fei, Y.Z. Cao, J. Yu, L.Y. Yuan, L. Gong, J. Chen, S.Z. Deng, J. Zhou, W.L. Guo, Water-evaporation-induced electricity with nanostructured carbon materials, Nat. Nanotech. 12 (4) (2017) 317–322.
[7] R.G. Picknett, R. Bexon, The evaporation of sessile or pendant drops in still air, J. Colloid Interface Sci. 61 (2) (1977) 336–351.
[8] Y.X. Li, P.Y. Lv, C. Diddens, H.S. Tan, H. Wijshoff, M. Verluis, D. Lohse, Evaporation-triggered segregation of sessile binary droplets, Phys. Rev. Lett. 120 (22) (2018) 224501.
[9] Y.S. Yu, L. Sun, X.F. Huang, J.Z. Zhou, Evaporation of ethanol/water mixture droplets on a pillar-like PDMS surface, Colloid Surf. A 574 (2019) 215–220.
[10] X.M. Chen, R.Y. Ma, J.T. Li, C.L. Hao, W. Guo, B.L. Luk, S.C. Li, S.H. Yao, Z.K. Wang, Evaporation of droplets on superhydrophobic surfaces: surface roughness and small droplet size effects, Phys. Rev. Lett. 109 (11) (2012) 116101.
[11] F.C. Wang, H.A. Wu, Pinning and depinning mechanism of the contact line during evaporation of nano-droplets sessile on textured surfaces, Soft Matter 9 (24) (2013) 5703–5709.
[12] Y.C. Chuang, C.K. Chu, S.Y. Lin, L.J. Chen, Evaporation of water droplets on soft patterned surfaces, Soft Matter 10 (19) (2014) 3394–3403.
[13] Y.S. Yu, X.F. Huang, L. Sun, J.Z. Zhou, A. Zhou, Evaporation of ethanol/water mixture droplets on micro-patterned PDMS surfaces, Int. J. Heat Mass Transf. 144 (2019) 118708.
[14] G. McHale, S. Aqil, N.J. Shirtcliffe, M.I. Newton, H.Y. Erbil, Analysis of droplet evaporation on a superhydrophobic surface, Langmuir 21 (24) (2005) 11053–11060.
[15] D.H. Shin, S.H. Lee, J.Y. Jung, J.Y. Yoo, Evaporating characteristics of sessile droplet on hydrophobic and hydrophilic surfaces, Microelectron. Eng. 86 (4–6) (2009) 1350–1353.
[16] Y. Wang, Z.G. Wang, Droplets wetting and evaporation on ethanol-philic micro-structured surfaces, Int. J. Heat Mass Transf. 119 (2018) 704–708.
[17] Y.S. Li, C.J. Lv, Z.H. Li, D. Quéré, Q.S. Zheng, From coffee rings to coffee eyes, Soft Matter 11 (23) (2015) 4669–4673.
[18] J.J. Zhang, H.B. Huang, X.Y. Lu, Pinning-depinning mechanism of the contact line during evaporation of nanodroplets on heated heterogeneous surfaces: a molecular dynamics simulation, Langmuir 35 (19) (2019) 6356–6366.
[19] G. Pu, S.J. Severtson, Water evaporation on highly viscoelastic polymer surfaces, Langmuir 28 (26) (2012) 10007–10014.
[20] M.C. Lopes, E. Bonaccurso, Evaporation control of sessile water drops by soft viscoelastic surfaces, Soft Matter 8 (30) (2012) 7875–7881.
[21] Y.S. Yu, Z.Q. Wang, Y.P. Zhao, Experimental study of evaporation of sessile water droplet on PDMS surfaces, Acta Mech. Sin. 29 (6) (2013) 799–805.
[22] G.J. Dunn, S.K. Wilson, B.R. Duffy, S. David, K. Sefiane, The strong influence of substrate conductivity on droplet evaporation, J. Fluid Mech. 623 (2009) 329–351.
[23] K. Sefiane, R. Bennacer, An expression for droplet evaporation incorporating thermal effects, J. Fluid Mech. 667 (2011) 260–271.
[24] S. Shyam, P.K. Mondal, B. Mehta, Field driven evaporation kinetics of a sessile ferrofluid droplet on a soft substrate, Soft Matter 16 (28) (2020) 6619–6632.
[25] D. Mampallil, H.B. Eral, D. van den Ende, F. Mugele, Control of evaporating complex fluids through electrowetting, Soft Matter 8 (41) (2012) 10614–10617.
[26] M.A. Kazemi, D.S. Nobes, J.A.W. Elliott, Experimental and numerical study of the evaporation of water at low pressures, Langmuir 33 (18) (2017) 4578–4591.
[27] T. Ozturk, H.Y. Erbil, Evaporation of water-ethanol binary sessile drop on fluoropolymer surfaces: influence of relative humidity, Colloid Surface A 553 (2018) 327–336.
[28] A. Lafuma, D. Quéré, Superhydrophobic states, Nat. Mater. 2 (7) (2003) 457–460.
[29] Q.Z. Yuan, X.F. Huang, Y.P. Zhao, Dynamic spreading on pillar-arrayed surfaces: viscous resistance versus molecular friction, Phys. Fluids 26 (9) (2014) 092104.
[30] E.H. Chen, Q.Z. Yuan, Y.P. Zhao, Topography-induced symmetry of droplets on quasi-periodically patterned surfaces, Soft Matter 14 (30) (2018) 6198–6205.
[31] R.N. Wenzel, Resistance of solid surfaces to wetting by water, Ind. Eng. Chem. 28 (8) (1936) 988–994.
[32] A.B.D. Cassie, S. Baxter, Wettability of porous surfaces, Trans. Faraday Soc. 40 (1944) 546–551.
[33] A. Tuteja, W. Choi, M.L. Ma, J.M. Mabry, S.A. Mazzella, G.C. Rutledge, G.H. McKinley, R.E. Cohen, Designing superolephobic surfaces, Science 318 (5856) (2007) 1618–1622.
[34] A. Marmur, Wetting on hydrophobic rough surfaces: to be heterogeneous or not to be? Langmuir 19 (20) (2013) 8343–8348.
[35] J. Bico, C. Marzolin, D. Quéré, Pearl drops, Europhys. Lett. 47 (2) (1999) 220–226.
[36] E. Bormashenko, R. Pogreb, G. Whyman, Y. Bormashenko, M. Erlich, Vibration-induced Cassie-Wenzel transition on rough surfaces, Appl. Phys. Lett. 90 (20) (2007) 201917.

[37] A. Sudeepthi, L. Yeo, A.K. Sen, Cassie-Wenzel wetting transition on nanostructured superhydrophobic surfaces induced by surface acoustic waves, Appl. Phys. Lett. 116 (9) (2020) 093704.
[38] P.C. Tsai, R.G.H. Lammertink, M. Wessling, D. Lohse, Evaporation-triggered wetting transition for water droplets upon hydrophobic microstructures, Phys. Rev. Lett. 104 (11) (2010) 116102.
[39] R. Chen, L. Jiao, X. Zhu, Q. Liao, D.D. Ye, B. Zhang, W. Li, Y.P. Lei, D.L. Li, Cassie–to-Wenzel transition of droplet on the superhydrophobic surface caused by light induced evaporation, Appl. Therm. Eng. 144 (2018) 945–959.
[40] C. Luo, M.M. Xiang, X.C. Liu, H. Wang, Transition from Cassie-Baxter to Wenzel states on microline-formed PDMS surfaces induced by evaporation or pressing of water droplets, Microfluid. Nanofluid. 10 (4) (2011) 831–842.
[41] H. Agogo, S. Semenov, F. Ortega, R.G. Rubio, V.M. Starov, M.G. Velarde, Spreading and evaporation of surfactant solution droplets, Progr. Colloid Polym. Sci. 139 (2012) 1–9.
[42] M.D. Doganci, B.U. Sesli, H.Y. Erbil, Difussion-controlled evaporation of sodium dodecyl sulfate solution drops placed on a hydrophobic substrate, J. Colloid Interface Sci. 362 (2011) 524–531.
[43] G.T. Barnes, The effects of monolayers on the evaporation of liquids, Adv. Colloid Interface Sci. 25 (1986) 89–200.
[44] W. Kwieciński, T. Segers, S. van der Werf, A. van Houselt, D. Lohse, H.J.W. Zandvliet, S. Kooij, Evaporation of dilute sodium dodecyl sulfate droplets on a hydrophobic substrate, Langmuir 35 (32) (2019) 10453–10460.
[45] A. Akanno, L. Perrin, E. Guzmán, S. Llamas, V.M. Starov, F. Ortega, R.G. Rubio, M.G. Velarde, Evaporation of sessile droplets of polyelectrolyte/surfactant mixtures on silicon wafers, Colloid Interface 5 (2021) 12.
[46] A. Marin, R. Liepelt, M. Rossi, C.J. Kähler, Surfactant-driven flow transitions in evaporating droplets, Soft Matter 12 (5) (2016) 1593–1600.
[47] G. Karapetsas, K.C. Sahu, O.K. Matar, Evaporation of sessile droplets laden with particles and insoluble surfactants, Langmuir 32 (27) (2016) 6871–6881.
[48] A. Aldhaleai, P.A. Tsai, Evaporation dynamics of surfactant-laden droplets on a superhydrophobic surface: linfluence of surfactant concentration, Langmuir 38 (1) (2022) 593–601.
[49] A. Carre, M.E.R. Shanahan, Drop motion on an inclined plane and evaluation of hydrophobic treatments to glass, J. Adhesion 49 (1995) 177–185.
[50] C.J. Lv, C.W. Yang, P.F. Hao, F. He, Q.S. Zheng, Sliding of water droplets on microstructured hydrophobic surfaces, Langmuir 26 (11) (2010) 8704–8708.
[51] Y. Yonemoto, S. Suzuki, S. Uenomachi, T. Kunugi, Sliding behavior of water-ethanol mixture droplets on inclined low-surface-energy solid, Int. J. Heat Mass Transf. 120 (2018) 1315–1324.
[52] N. Gao, F. Geyer, D.W. Pilat, S. Wooh, D. Vollmer, H.J. Butt, R. Berger, How drops start sliding over solid surfaces, Nat. Phys. 14 (2) (2018) 191–196.
[53] C.W. Yao, S.R. Tang, D. Sebastian, R. Tadmor, Sliding of water droplets on micropillar-structured superhydrophobic surfaces, Appl. Surface Sci. 504 (2020) 144493.
[54] T. Huhtamäki, X.L. Tian, J.T. Korhonen, R.H.A. Ras, Surface-wetting characterization using contact-angle measurements, Nat. Protoc. 13 (7) (2018) 1521–1538.
[55] E. Bormashenko, Y. Bormashenko, G. Whyman, R. Pogreb, A. Musin, R. Jager, Z. Barkay, Contact angle hysteresis on polymer substrates established with various experimental techniques, its interpretation, and quantitative characterization, Langmuir 24 (8) (2008) 4020–4025.
[56] Q.S. Zheng, Y. Yu, Z.H. Zhao, Effects of hydraulic pressure on the stability and transition of wetting modes of superhydrophobic surfaces, Langmuir 21 (26) (2005) 12207–12212.
[57] J.L. Liu, Y. Mei, R. Xia, A new wetting mechanism based upon triple contact line pinning, Langmuir 27 (1) (2011) 196–200.
[58] G. Whyman, E. Bormashenko, How to make the Cassie wetting state stable? Langmuir 27 (13) (2011) 8711–8716.
[59] L. Barbieri, E. Wagner, P. Hoffmann, Water wetting transition parameters of perfluorinated substrates with periodically distributed flat-top microscale obstacles, Langmuir 23 (4) (2007) 1723–1734.
[60] N.A. Patankar, Consolidation of hydrophobic transition criteria by using an approximate energy minimization approach, Langmuir 26 (11) (2010) 8941–8945.